Lacustrine Shale Diagenesis—A Case Study of the Second Member of the Funing Formation in the Subei Basin

Shuping Wang [1,*], Cunfei Ma [2], Xue Sun [2] and Shili Liu [3]

1   Petroleum Industry Training Center, China University of Petroleum (East China), Qingdao 266580, China
2   School of Geosciences, China University of Petroleum (East China), Qingdao 266580, China; mcf-625@163.com (C.M.)
3   Geological Scientific Research Institute of Jiangsu Oilfield, SINOPEC, Yangzhou 225009, China
*   Correspondence: wshp0619@163.com

Abstract: Shale diagenesis differs from that of sandstone and carbonate rocks with regard to the type, evolution stage, and evolution mode. The quality of shale reservoirs is closely linked to the extent of diagenetic evolution. This study identifies the types and characteristics of shale diagenesis using thin sections and scanning electron microscopy (SEM) observations. The stages of shale diagenesis are determined by analyzing organic matter evolution and clay mineral transformation and establishing a diagenetic evolution sequence. This paper describes the comprehensive diagenetic evolution of organic matter, clay minerals, clastic particles, and carbonate minerals to determine the diagenesis types, diagenetic sequences, and pore evolution occurring during diagenetic evolution. The results show that the diagenesis types of shale in the second member of the Funing Formation include compaction, dissolution, cementation, metasomatism, dolomitization, syneresis, and transformation of clay minerals, as well as thermal evolution of organic matter. The middle diagenetic A stage is prevalent, with some areas in the early and middle diagenetic B stages. The shale underwent a diagenetic evolution sequence, including the collapse and shrinkage of montmorillonite interlayers in the early stage; the rapid formation and transformation of illite and smectite mixed layers, massive hydrocarbon generation of organic matters, and dissolution of unstable components in the middle stage; and the occurrence of fractures filled with gypsum, quartz, ferrocalcite, or other authigenic minerals in the later stage. Dissolution pores and fractures are the dominant shale reservoirs of the second member of the Funing Formation in the Subei Basin. The results provide new insights into understanding the formation and evolution of reservoir spaces during shale diagenesis and information for the exploration and development of lacustrine shale oil and gas.

Keywords: shale; diagenesis type; diagenetic stage; diagenetic evolution sequence; pore evolution

1. Introduction

Shale diagenesis is a complex process with various physical, chemical, and biological effects between sediment deposition and metamorphism [1–3]. The mineral composition in shale is intricate and delicate, making it highly sensitive to temperature, pressure, and fluid activity fluctuations. Additionally, clay mineral dehydration and organic hydrocarbon generation heighten fluid activity, resulting in a strong heterogeneity in shale reservoirs. Dissolution, cementation, and metasomatism are more intricate in shale than in sandstone and carbonates. Therefore, the mechanism of burial diagenesis transformation is more intricate in shale than in other reservoirs. As geologists have focused more on unconventional oil and gas exploration and development, shale reservoirs have become increasingly important [4–8].Shale diagenesis influences several shale characteristics, such as its sedimentary structure, material composition, reservoir physical and mechanical properties, and the generation and preservation of pores [9,10]. Consequently, diagenesis is critical in controlling oil and gas generation, migration, and concentration, and the exploration

and development of shale oil and gas resources [11,12]. Therefore, many scholars have recognized the significance of shale diagenesis research for the optimal exploration and development of shale oil and gas resources [13–18].

Research on the diagenesis of marine shale comprises various aspects, including mudstone compaction and its effect on the microstructure and properties of rock [19,20], the transformation of clay minerals and siliceous cementation during burial [21,22], the identification and progression of the quartz source in marine silica shale (Milliken et al., 2016), the formation and dissolution of secondary pores in shale reservoirs [23], the role of the initial composition of the shale material on its diagenetic path [24], and the organogenesis in shale reservoirs [25]. On the other hand, the main focus of research on the diagenesis of lacustrine shale has been shale diagenesis and the evolution of reservoir pores in formations such as the Lucaogou Formation in the Malang Sag and the Paleogene of the Jiyang Depression [26–28].

The current focal points in shale diagenesis research include examining changes in the mechanical properties during the thermal evolution of organic matter, spatially characterizing underground diagenetic cementation belts, exploring the impact of diagenesis on the mechanical and reservoir properties of shale reservoirs, analyzing the influence of initial material composition on mudstone compaction, identifying the original clastic materials and possible diagenetic evolution paths in mudstones, and studying fine-grained deposition and its influence on diagenesis [18]. The ultimate goal of shale diagenesis research is to discern the spatial characterization of diagenetic facies zones by obtaining a comprehensive understanding of shale diagenetic evolution and its effects on reservoir properties. One key approach to accomplish this is to investigate the initial material composition and its impact on diagenetic evolution from a sedimentation perspective. The initial material composition, bedding structure, oxygen content, chemical properties, and biological productivity of shale depend on sedimentation and the sedimentary environment, which can substantially affect several biochemical reactions, compaction processes, and subsequent thermochemical reactions that occur during sediment burial [24,29–31].

The shale strata in lake basins hold great potential for oil and gas exploration. However, due to the high variability of salinization in different lake basins, the diagenesis of these strata is quite complex and specific; thus, further research is required to understand it fully [32]. Current research has focused on the transformation of clay minerals during diagenesis, but there is no unified standard for dividing the different stages of shale diagenesis and no clear understanding of the diagenetic evolution sequence of the shale's components [33–35]. This study aims to address this gap by analyzing a typical continental lake shale in the second member of the Funing Formation (Fu-2) to refine the shale diagenetic stages, establish a diagenetic evolution sequence and model, and summarize the pore evolution. We provide a novel method for shale diagenesis studies to improve the comprehension of the formation and evolution of reservoir spaces during shale diagenesis. The findings can be used for the future exploration and development of lacustrine shale oil and gas.

2. Overview of the Study Area

The Subei Basin is the terrestrial part of the Subei–South Yellow Sea Basin. It is located between Jiangsu Province and Anhui Province in eastern China, north of the Yangtze River in Jiangsu Province, and extends to the Yellow Sea. It covers an area of about 3.5×10^4 km². The basin borders the Lusu uplift to the north, Zhangbaling uplift to the south, Tanlu fault to the west, and Yellow Sea to the east. It is a Mesozoic–Cenozoic continental basin developed on the Lower Yangtze activated platform. The Subei Basin consists of four sags: the Haian sag, Gaoyou sag, Jinhu sag, and Yancheng sag, from east to west (Figure 1). The Funing Formation was formed during the Paleogene in the Subei Basin in a fault–depression tectonic cycle. The Fu-2 in the Subei Basin is located in the transgressive system tract of the secondary sequence or the highstand system tract of the lake. It is a complete third-order sequence. Numerous organisms and extensive lacustrine sediments exist because

of the continuous subsidence of the basin and the injection of terrigenous clasts. Many layers of thick, dark shale were deposited in the deep lake during a period of intense fault–depression activity. The aqueous medium is semisaline, weakly alkaline, and strongly reductive. The Funing Formation can be divided into four sections, from bottom to top: the first, second, third, and fourth members of the Funing Formation (Fu-1, Fu-2, Fu-3, and Fu-4). The upper part of Fu-1 consists primarily of delta front sub-facies, Fu-2 comprises coastal and shallow lake subfacies, Fu-3 consists of delta front subfacies, and Fu-4 contains predominantly lake facies [36,37]. The lithologic assemblages of Fu-2 include thin interbeds of shale, marl, and dolomite.
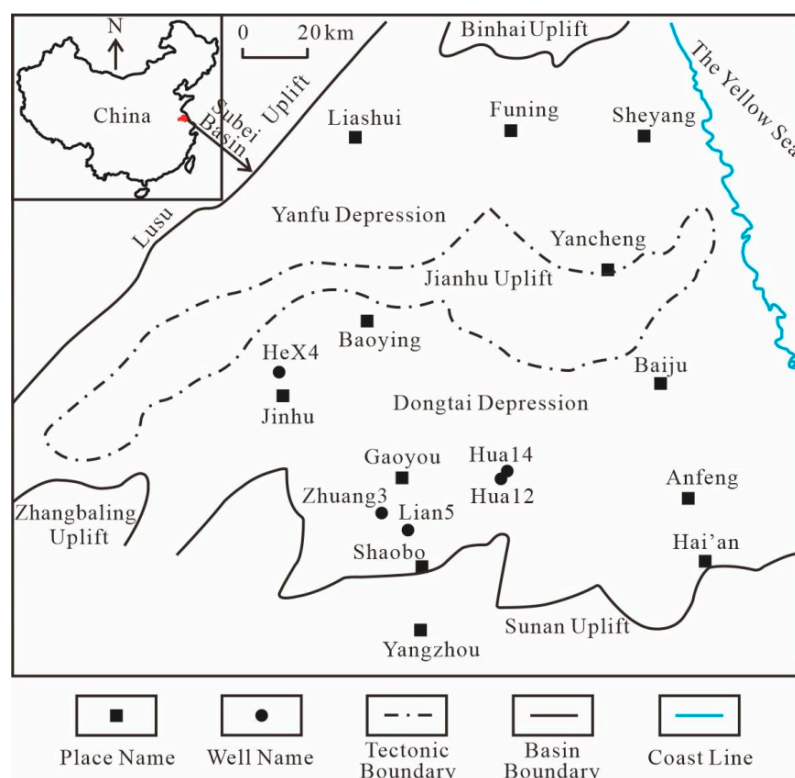

Figure 1. Structural units of the Subei Basin.

3. Methods

A total of 300 shale samples were selected according to the shale facies type and burial depth to grind ordinary thin sections. The mineral composition and distribution, organic matter distribution, bio-fossil type and characteristics, micro-bedding type, diagenesis type, and fracture type and characteristics were observed using a Zeiss Axio Scope A1 pol polarizing microscope at the Key Laboratory of Marine Reservoir Evolution and Hydrocarbon Accumulation of the China University of Geosciences (Beijing, China). The samples were cut into blocks of approximately 1 cm^3 and ground, and secondary electron imaging (SE) and backscattered electron imaging (BSE) were conducted at an accelerating voltage of 2–10 kV. The microscope was equipped with a high-quality optical system, including color aberration correction, automatic brightness compensation, spherical aberration correction, and other functions. The thin sections were observed at high resolution and high contrast.

The mineral grains in the shale were small, generally less than 62.5 μm, and the dominant pore sizes were micropores and nanopores. The maximum magnification of optical microscopy is typically 500×, too small to observe the shale's microcharacteristics. However, the resolution of scanning electron microscopy (SEM) can reach 0.3 nm, enabling microstructure observations. Since Loucks first used argon ion polishing to treat Barnett shale samples and utilized SE and BSE in field emission scanning electron microscopy (FE-SEM) combined with energy dispersive spectroscopy (EDS) to observe the size and

distribution of nanopores in shale, FE-SEM has become a necessary method for studying shale microstructure [5,7,38–40]. A Quanta 200F field emission scanning electron microscope was used to observe the shale samples polished by a Gatan697 Ilion II broad-beam argon ion polishing system to study the types and microcharacteristics of minerals and organic matter, diagenesis types, reservoir space types, and diagenetic evolution.

X-ray diffraction (XRD) is an effective method to quantify shale mineral composition and perform whole-rock mineral and clay mineral analyses to determine the lithofacies type and diagenesis [41–43]. The samples were ground to a fine powder, dried, and pressed through a sieve, and the elements of 32 samples were quantified using X-ray fluorescence spectrometry (SPECTRO). An X'Pert PRO MPD diffractometer was used at the Key Laboratory of Orogenic Belts and Crustal Evolution at Peking University, and X'Pert HighScore software 2.2a was used to analyze the type and content of clay minerals in the shale. The clay mineral evolution was determined by calculating the ratio of illite and smectite in mixed layers to obtain the diagenesis stages.

Organic geochemical testing is commonly used in source rock evaluation [44,45]. Organic matter is the main component of shale and is sensitive to temperature and pressure. Therefore, organic geochemical parameters reflecting the thermal evolution of organic matter can be used to indicate the shale's diagenetic evolution. The color and thermodynamic index (TAI) of the sporopollenin and the kerogen vitrinite reflectance (Ro) were determined using thin sections, a transmission light microscope, and an MVP-SP microscope photometer [46]. Before the experiment, 10% hydrochloric acid was used to remove carbonates; the test sensitivity was 10–13 mg/g. The peak temperature (Tmax) was measured using a GHM-02 hydrocarbon analyzer [47]. The hydrocarbons derived from the shale pyrolysis experiments were analyzed by an HP 6890 gas chromatograph. The carbon preference indices (CPIs) of the n-alkanes were obtained [48]. Additionally, measurements were obtained to determine the isolated kerogen content and identify the organic kerogen macerals, carbon isotope content, and organic element content according to the (GB/T) 19144e2010, (SY/T) 5125e2014, (GB/T) 18340.2e2010, and (GB/T) 19143-2003 standards, respectively. The kerogen measurements and the rock pyrolysis analysis were performed at the Keyuan Engineering Technology Testing Center.

4. Results

4.1. Shale Petrological Characteristics

Compositionally, the shale in the Fu-2 in the North Jiangsu Basin is fine-grained, mixed, and temperature/pressure sensitive, and it has an active fluid system. It contains fine-grained felsic minerals (silt or very fine silt), clay minerals, carbonate minerals, and organic matter [27]. The genesis of the shale's components is complex and is influenced by multiple factors. For example, silt and clay minerals are formed by mechanical deposition and are transformed by diagenesis at a later stage (Figure 2). Calcite and dolomite in carbonate minerals are of syngenetic or quasi-syngenetic chemical sedimentary origin, whereas iron calcite and iron dolomite are formed during diagenesis. Organic matter has a biogenic origin and is predominantly generated by plankton in the basin; examples include collophanite and calcareous or siliceous microfossils. Pyrite, siderite, galena, sphalerite, gypsum, and barite have a more diverse genesis, and multiple genesis types can occur in the same shale sample (Figure 2). Pyrite and siderite typically originate in an organic-rich environment that releases acidic elements during decomposition. This process etches the minerals and creates shale pores. When plaster dissolves in an aqueous solution, it forms tiny karst caverns and channels that can serve as pores and reservoirs for shale. In addition, hydrothermal minerals such as zeolite can form in magma in active tectonic areas (Figure 2). Zeolite has excellent catalytic performance, promoting the pyrolysis and transformation of organic matter in shale. Hydrocarbon generation by organic matter pyrolysis creates organic pores. The acidic fluids produced by organic matter pyrolysis dissolve minerals such as feldspar and calcite, forming dissolution pores and increasing the shale's storage capacity and permeability.
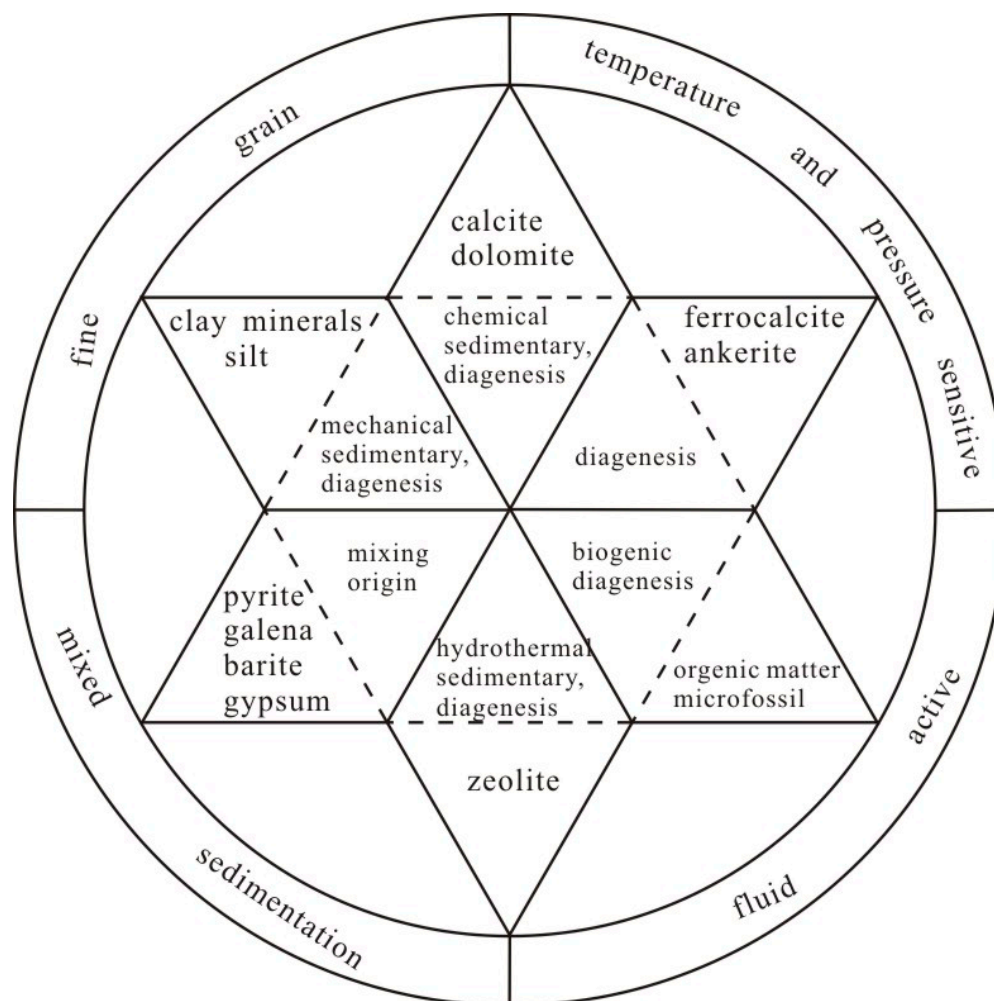
Figure 2. Components of the E_1f_2 shale and their genesis.

The debris particles in the shale are not randomly distributed but generally exhibit features parallel to the layers, showing three types of microscopic bedding patterns: sheets, directional orientation, and blocks (Figure 3). The sheetlike microscopic bedding is composed of argillaceous, calcareous, or fine interbedded layers rich in organic matter, and the layer interface is clear, straight, and continuous. Microscopic bedding with a directional orientation consists of strips of argillaceous, carbonaceous, organic, bioclastic, or terrigenous clasts, and the interfacial layers are intermittent or unclear. The microscopic bedding with blocks is characterized by a uniform distribution or an indistinct directional orientation of the components. A lamellar bedding pattern is formed by the hydrodynamic force and gravity in the sedimentary environment. Many parallel planes exist in the horizontal direction, and the angle between these planes is small, usually from 1 to 10 degrees. The laminates exhibit cohesiveness, limiting the expansion and development of pores and affecting the shale's permeability. The directional bedding pattern is formed by hydrodynamic action in the sedimentary environment, and the dip angle of the plane is generally between 10 and 30 degrees. The pore connectivity is high, and the pore distribution is relatively uniform. The pores are aligned in the plane's inclination direction, and the pore size is affected by the plane's inclination angle. The blocky bedding pattern is formed by gravity in the sedimentary environment, and large blocky rock masses with large angles occur, usually between 30 and 90 degrees. The pores are often unevenly distributed between the rock masses, and their connectivity is low.
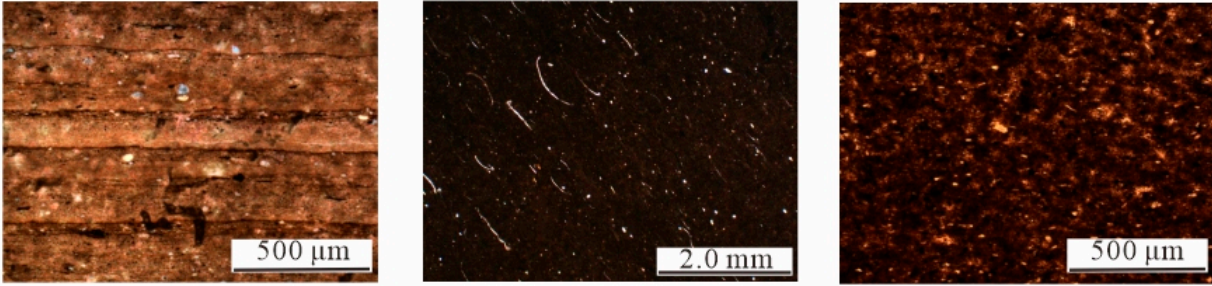
Micro-bedding type	Sheet	Directional	Block
bedding characteristics	fine interbedding of argillaceous, calcareous layer or organic rich layers; the lamina interface is clear, straight and continuous	directional arrangement or strip distribution of argillaceous, carbonaceous, organic, bioclastic or terrigenous clasts, and the interfacial layers are intermittent or not obvious	uniform distribution or indistinct directional arrangement
bedding continuity	continuous	discontinuous	no

500 μm	2.0 mm	500 μm
continuous sheet type Sha 20 well, 2192.10m	discontinuous directional type Lian 5 well, 2343.6m	uniform distribution type Xinzhu 1 well, 2714m

Figure 3. The types of microscopic stratifications of the E_1f_2 shale.

4.2. Types of Shale Diagenesis

Shale contains the dominant minerals comprising sandstone and carbonate rock, as well as clay minerals and organic matter. Due to temperature and pressure, the fluid generated by clay minerals and organic matter interacts with the rock skeleton, producing various types of diagenesis, including compaction, dissolution, cementation, and metasomatism [26], dolomitization in carbonate rocks, dehydration, shrinkage, and transformation of clay minerals in clay rocks, and the unique thermal evolution of organic matter.

4.2.1. Compaction

After the sediment has been deposited, the overlying strata pressure increases with the burial depth. The water in the intergranular pores of the clastic particles and mineral intercrystalline pores is continuously discharged, and the shale volume decreases due to compaction. Compaction is the most common type of diagenesis in shale. Typical phenomena are the directional orientation of long clastic particles, bending deformation of plastic minerals, fragmentation of brittle minerals, or compression into plastic argillaceous laminae. Pressure solution can be observed in lime laminae with a high carbonate mineral content (Figure 4).

4.2.2. Dissolution

Dissolution in shale is an important diagenesis type, especially in organic-rich shale. Organic acids produced by the maturation of organic matter cause the dissolution of unstable components during their transportation. Calcite (Figure 5A–C) and feldspar (Figure 5D) are the main unstable components of dissolution in the Fu-2. The dissolution of pyrite (Figure 5E) or zeolite (Figure 5F) can also be observed in some samples. The acidic fluid dissolves the particles along the edge, cleavage, or microcrack, forming intergranular or intragranular dissolution pores (Figure 5).
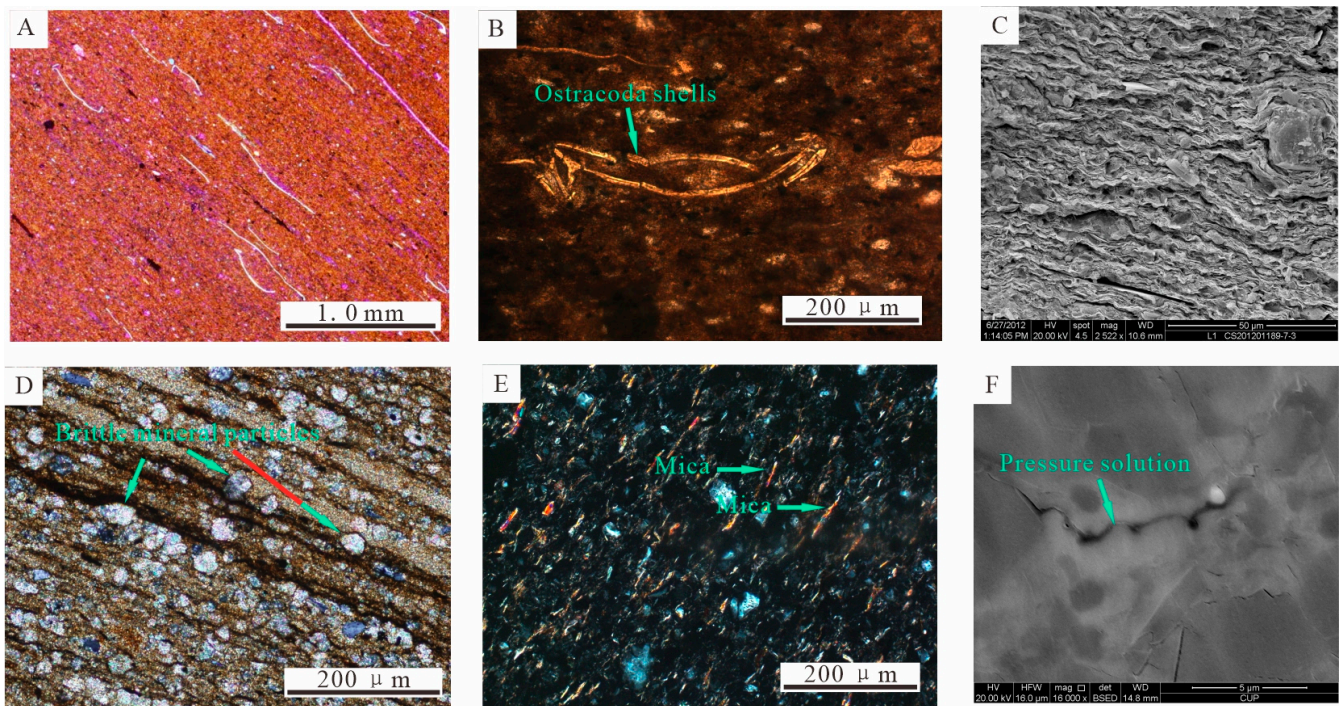
Figure 4. The compaction of the E_1f_2 shale. (**A**) Directional orientation of Ostracoda shells, Yancan 1, 3008.77 m; (**B**) crushed Ostracoda shells, Xinzhu 1, 2714 m; (**C**) bending deformation of plastic clay minerals, Lin 1, 2601.04 m; (**D**) brittle mineral particles are pressed into plastic argillaceous laminae, An 16, 3671.4 m; (**E**) directional orientation of mica, Xinzhu 1, 2912.18 m; and (**F**) pressure solution of carbonate minerals, Dan 1, 2100.85 m.
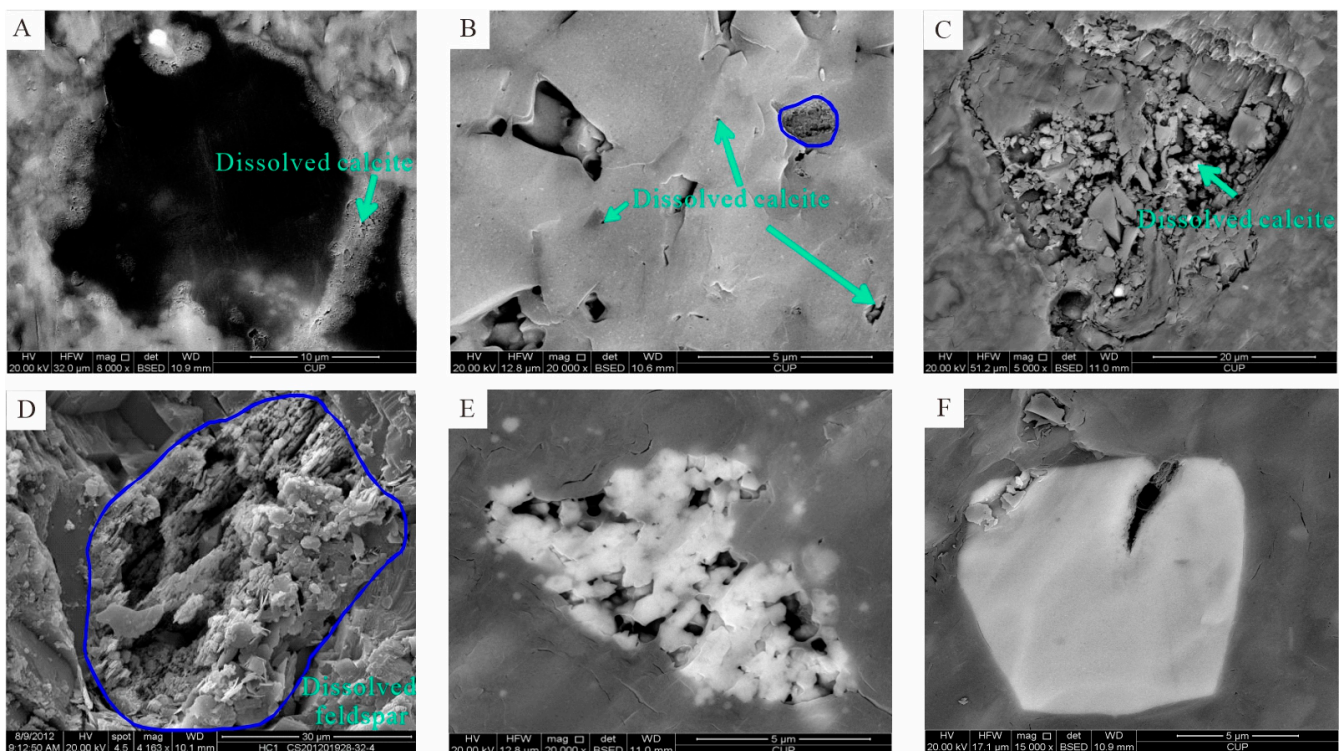

Figure 5. Dissolution of the E_1f_2 shale. (**A**) Dissolved calcite, 2302.6 m; (**B**) dissolved calcite, An16, 3669.8 m; (**C**) dissolved calcite, Lin1, 2601.87 m; (**D**) dissolved feldspar, Hecan1, 3164.77 m; (**E**) dissolved pyrite, Hexie4, 2302.6 m; and (**F**) dissolved zeolite, Sha31, 2740.52 m.

4.2.3. Cementation

When the fluid carrying dissolved diagenetic components migrates in the pore throat network or fractures of the shale, authigenic minerals precipitate and fill the reservoir space due to a change in the flow rate or chemical equilibrium reaction. Cements develop primarily in cracks and larger pores, and the crystal morphology is well-developed. There are various types of cements in the Fu-2, including sulfide (pyrite), sulfate (gypsum), carbonate (calcite or iron calcite), and siliceous materials (authigenic quartz and chert) (Figure 6). Pyrite is widely distributed and has various aggregate forms, such as dispersed spheres, strawberry-shaped particles, filaments, bands, or massive shapes (Figure 6A). Gypsum occurs predominantly as fillings (complete or semicomplete) of pores and fractures; sometimes it is dense, with a high content (Figure 6B). Carbonate cements mostly occur in shale facies with a high silt content, cementing sandy particles or filling intergranular pores (Figure 6C). Similar to carbonate cements, authigenic quartz in siliceous cements fills holes or cracks in a perfectly crystalline form (Figure 6D).
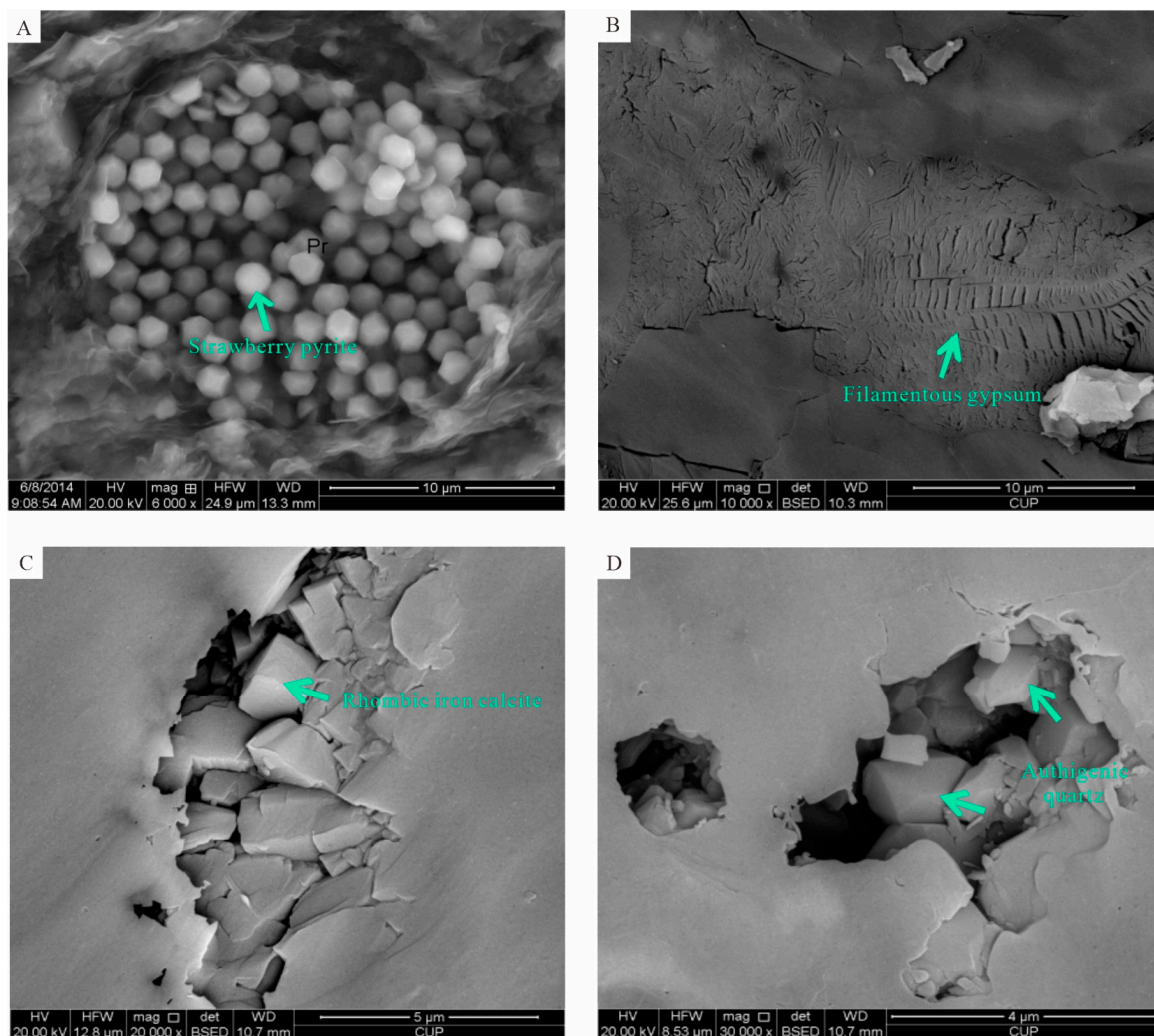

Figure 6. The cementation of the E_1f_2 shale. (**A**) Pyrite cementation with strawberry shapes, Huaxie 28, 3653.75 m; (**B**) gypsum cementation with filaments, Ma 1, 1743.14 m; (**C**) iron calcite cementation with a rhombohedral shape, Hexie 4, 2302.6 m; and (**D**) authigenic quartz cementation with cylindrical cones, Huaxie 28, 3655.5 m.

4.2.4. Metasomatism

Metasomatism can occur at all stages of diagenesis. Unlike sandstone and carbonate metasomatism, shale metasomatism is difficult to observe. Metasomatism in the Fu-2

involves primarily calcite (Figure 7A), iron calcite (Figure 7B), or pyrite-altering quartz (Figure 7C,D). The reason is that shale has a high degree of compactness and microscopic porosity, making it difficult for fluids to enter. In addition, the content of organic matter in shale is high, and the interaction between the organic matter and fluid can affect the metasomatism of shale.
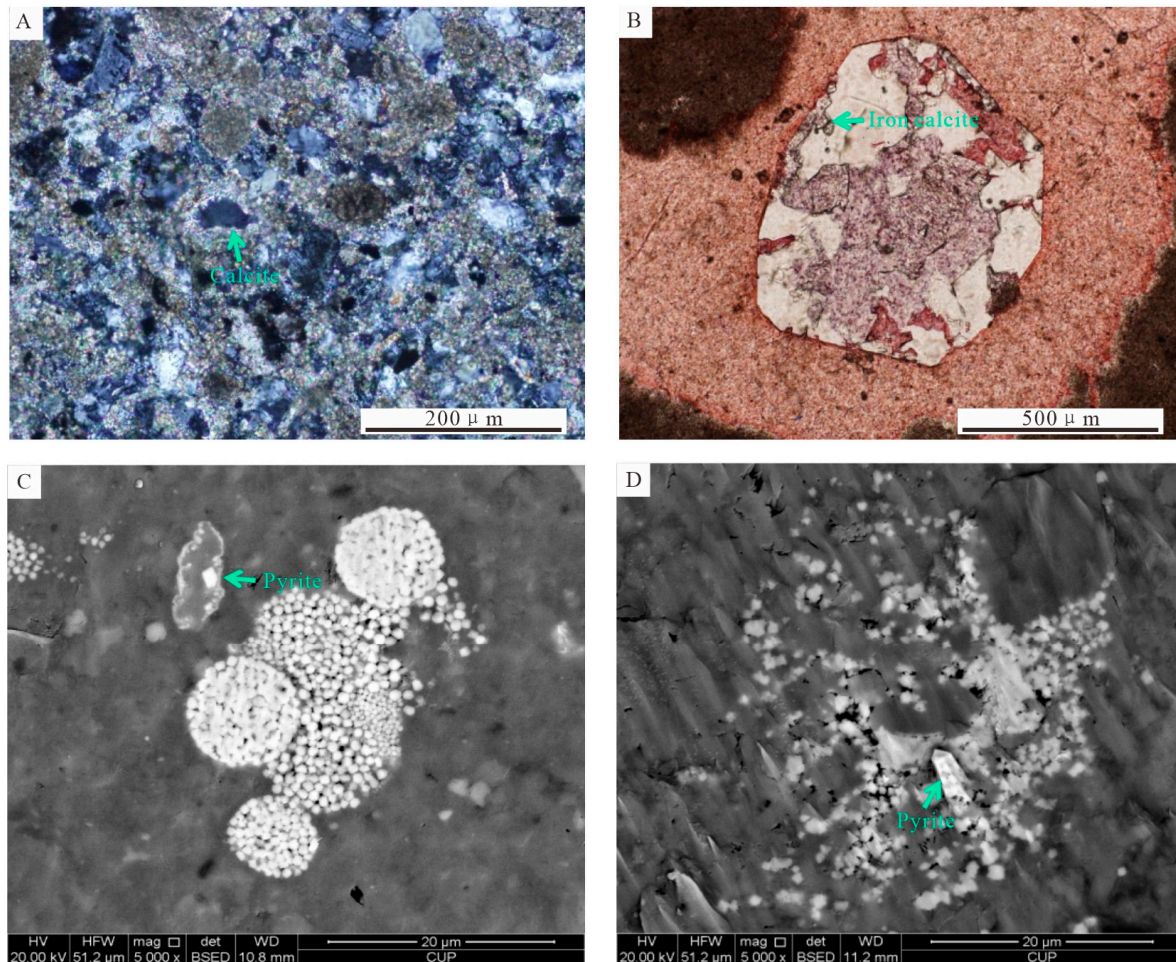

Figure 7. The metasomatism of the E_1f_2 shale. (**A**) Quartz metasomatized by calcite, An 1, 2687.3 m; (**B**) quartz metasomatized by iron calcite, Yancan 1, 3060 m; (**C**) quartz metasomatized by pyrite, Hexie 4, 2302.6 m; and (**D**) quartz metasomatized by pyrite, Huaxie 28, 3655.5 m.

4.2.5. Dolomitization

Dolomitization is commonly observed in shale facies with a high carbonate mineral content, forming rhombohedral dolomite particles that occur in isolation or are aggregated into laminae, resulting in granular or intercrystalline pores (Figure 8).

4.2.6. Dehydration/Shrinkage and Transformation of Clay Minerals

Clay minerals significantly affect shale structure and diagenetic evolution [49]. As the burial depth increases, higher temperatures and pressures cause clay minerals to absorb interlayer water and ions, generating fluids. As a result, the clay minerals are transformed from montmorillonite to illite or chlorite (Figure 9A,B,E,F)[50]. In addition, the orderliness of the clay minerals improves, and the volume is increased, resulting in shrinkage joints. When magmatic rocks, such as basalt or diabase, are transformed into shale, they lose a significant amount of water at high temperatures in a short time (Figure 9C,D). Shale undergoes shrinkage and thermal contact metamorphism, and cracks occur due to the excessive pressure of the hydrothermal fluid.
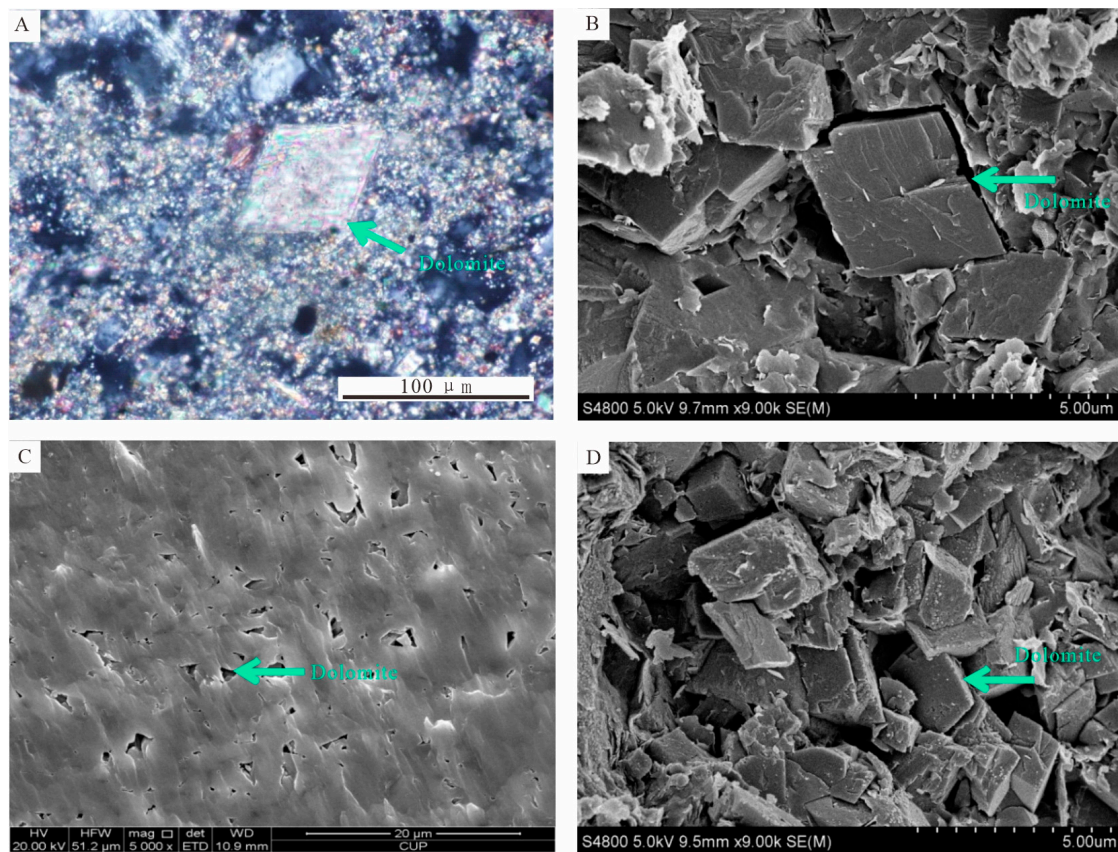
Figure 8. The dolomitization of the E_1f_2 shale. (**A**) Sha 31, 2741.74 m; (**B**) An 1, 2550.5 m; (**C**) Hexie 4, 2302.6 m; and (**D**) Ma 1, 1743.64 m.
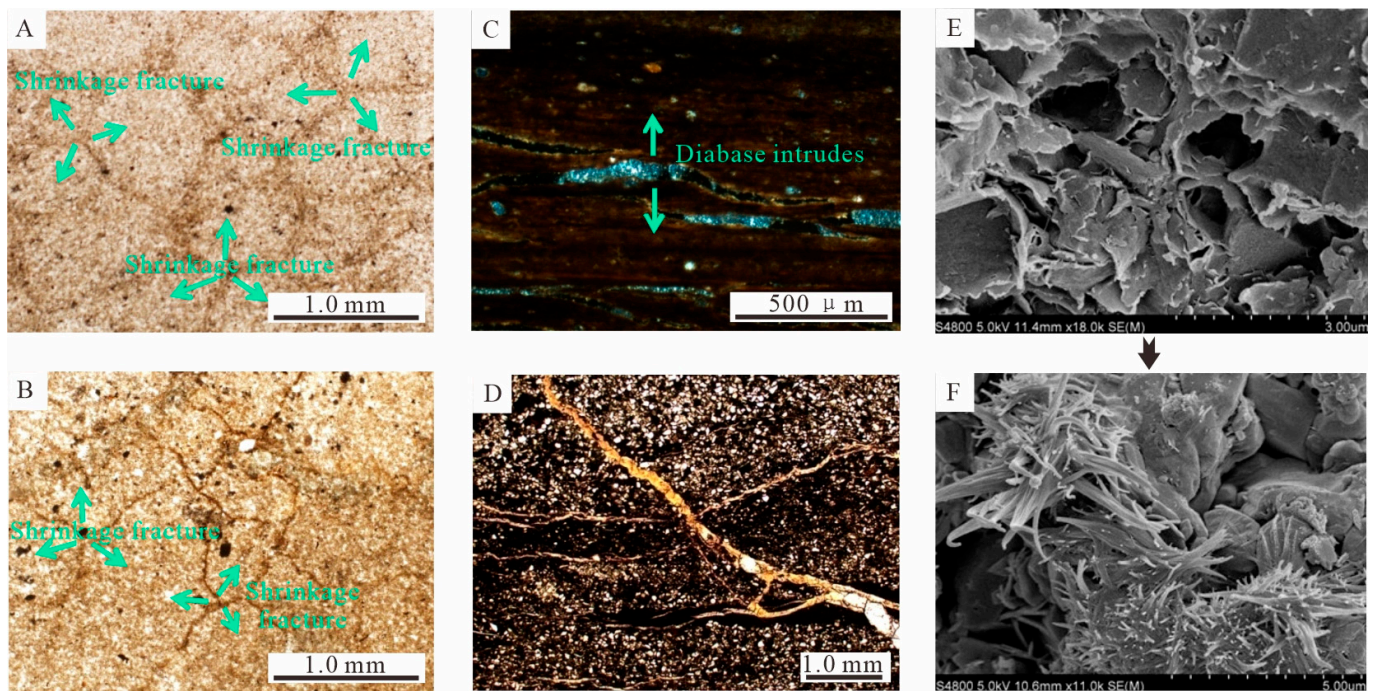

Figure 9. The syneresis and transformation of clay minerals of the E1f2 shale. (**A,B**) Shale shrinkage fracture caused by clay mineral dehydration and shrinkage, Fa 2, 2187.7 m; (**C,D**) diabase intrusion: shale undergoes low-grade thermal contact metamorphism, forming cracks, Sha 20, 2184.25 m; (**E**) lamellar montmorillonite, Sha 20, 2183.9; and (**F**) filamentous illite, Ma 1, 1743.64 m.

4.2.7. Thermal Evolution of Organic Matter

Organic matter is an essential component of shale, and its volume fraction can reach 32% in the Fu-2. Similar to clay minerals, organic matter is also sensitive to temperature and pressure, generating organic acids and hydrocarbons, another source of fluid generation in shale. Therefore, organic matter can be regarded as a unique component of shale, and the thermal evolution of organic matter can be regarded as a unique diagenesis type that differs from sandstone and carbonate rock diagenesis. As the Ro increases, organic matter matures and is converted into hydrocarbons, and numerous organic-matter pores are produced in the residual organic matter. The size and shape of these pores change constantly (Figure 10).
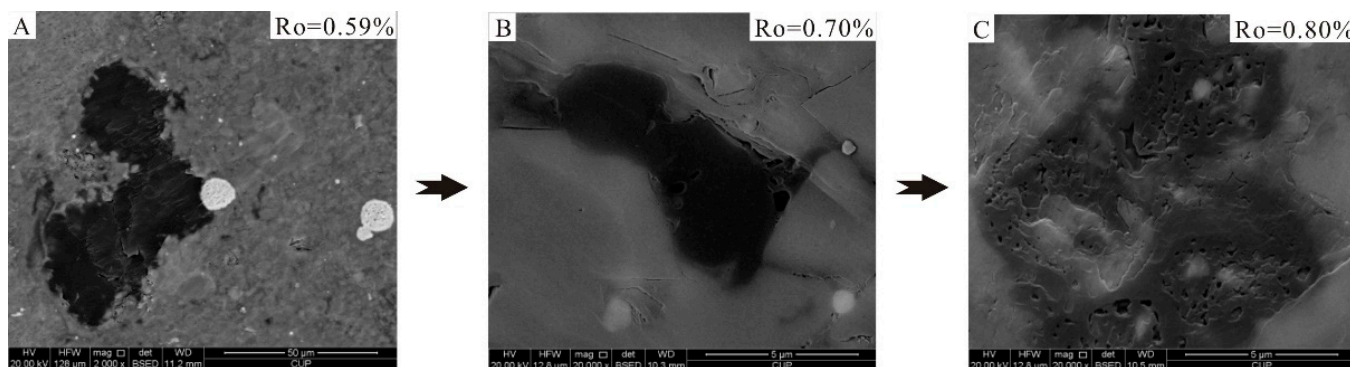

Figure 10. Changes in the size and shape of organic pores during the thermal evolution of organic matter in the E_1f_2 shale. (**A**) Lin 1, 2601.87 m; (**B**) Lin 1, 2730.43 m; and (**C**) Huaxie 28, 3653.75 m.

5. Discussion

5.1. Diagenetic Stages of Shale

The contents of organic matter and inorganic minerals in the shale reflect the diagenesis intensity of shale, which changes with the physical and chemical conditions during burial [12]. The organic matter and inorganic minerals are independent and interact during diagenetic evolution [11]. Therefore, the diagenetic stages are divided according to the diagenetic evolution characteristics in this paper.

5.1.1. Thermal Evolution of Organic Matter

The degree of the thermal evolution of organic matter is crucial for the division of the diagenetic stages of organic-rich shale. The main parameters that characterize the thermal evolution of organic matter are the Ro, CPI, Tmax, and other parameters. The diagenetic stages of the shale are determined according to the parameter range (Table 1).

Table 1. The relationship between the organic maturation index and the diagenetic stage [50].

Diagenetic Stage			Organic Matter Maturity	*Ro*%	*Tmax*/°C	Pollen Color	TAI
Early	**A**		Immature	<0.35	<435	Yellow	<2
	B		Semimature	0.35–0.5		Deep yellow	<2.5
Middle	A	A1	Low maturity	0.5–0.7	435–440	Orange	2.5–2.7
		A2	Mature	0.7–1.3	440–460	Brown	2.7–3.7
	B		High maturity	1.3–2.0	460–480±	Dark brown–black	3.7–4
Late			Post-mature	2.0–4.0	500±	Black	>4

The depth of shale in the Fu-2 ranges from 1000 m to 4000 m. The Ro is 0.45–0.9% (Figure 11A), and the Tmax is 430–450 °C (Figure 11B). The CPI decreases logarithmically during the thermal evolution and tends to 1, indicating parity equilibrium (Figure 11C). Accordingly, the organic matter maturity of the Fu-2 is low to mature, and the shale is in the middle diagenetic stage A.
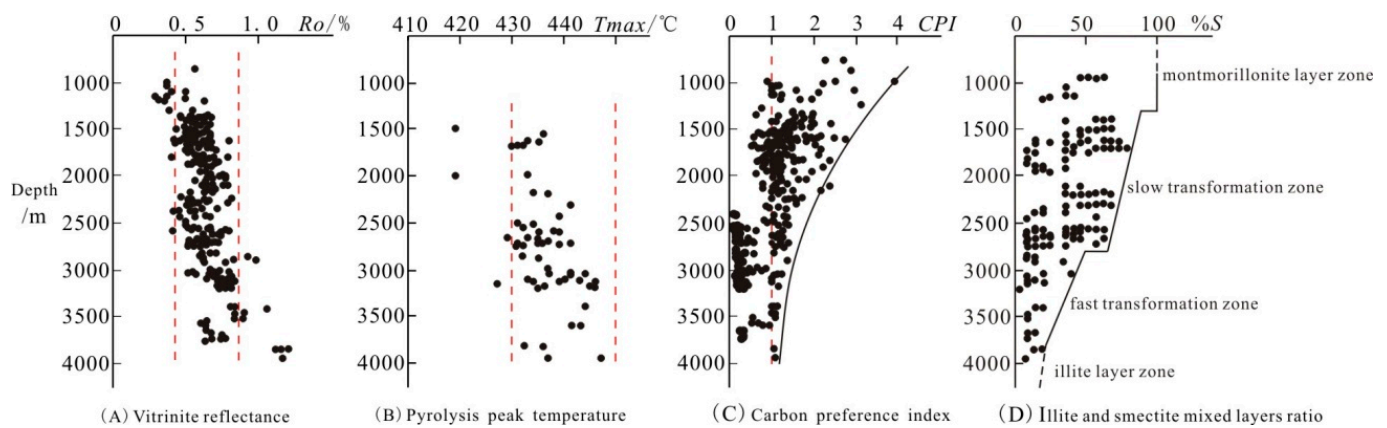
Figure 11. The thermal evolution of organic matter and the transformation of clay minerals of the E1f2 shale.

5.1.2. Clay Mineral Transformation

The transformation of clay minerals is crucial for determining the diagenetic stages. The types and transformation characteristics of the mixed illite and smectite layers are widely used [51,52]. Zoning is observed during the transformation of the illite and smectite mixed layers in the Fu-2 in the North Jiangsu Basin. According to the change in the content of the montmorillonite layer (S%) with the depth, four zones are observed: the montmorillonite layer, slow transformation zone, fast transformation zone, and illite layer. The main body of the shale in the study area is in the slow and fast transformation zones (Figure 11D). In conjunction with the thermal evolution index of organic matter (Figure 11A–C), it is determined that the middle diagenetic stage A is the dominant stage of the Fu-2 in the Subei Basin, with some areas in the early diagenetic stage B and the middle diagenetic stage B. The details are as follows.

Some shale samples of the Fu-2 in the montmorillonite zone are buried less than 1300 m, and the montmorillonite layer is dominant in the mixed illite and smectite layers. The Ro is less than 0.5%, the organic matter is immature or semimature, and the early diagenetic stage B is prevalent [21]. The shale burial depth in the slow transformation zone ranges from 1300 m to 2800 m. The montmorillonite content varies substantially, and the average content exceeds 50%; however, the montmorillonite has begun to transform into the mixed illite and smectite layers. The Ro is 0.5–0.7%, the organic matter maturity is low, and the middle diagenetic stage A1 occurs [31]. The shale burial depth in the fast transformation zone is 2800–3800 m, the montmorillonite content is substantially lower (35%), the Ro is 0.7–1.0%, and the organic matter is mature, indicating the middle diagenetic A2 stage [46]. Only a few samples with a buried depth greater than 3800 m were obtained. The average montmorillonite content is about 15%. The samples were obtained from the illite layer. The Ro is larger than 1.1%, and the organic matter is highly mature, indicating the middle diagenetic stage B.

5.2. Diagenetic Evolution Sequence of Shale

Based on the shale diagenetic events and the diagenetic stages, the diagenetic evolution sequence of the Fu-2 is established by describing the organic matter maturity and the contents of the clay, felsic, and carbonate minerals in the diagenetic stages.

The temperature, pressure, and fluid properties change during shale burial, altering the dynamic balance of the diagenetic environment, creating new diagenetic stages, and generating new diagenetic events. In the early stage of shale sedimentation, clay minerals mixed with fine-grained clastic particles are deposited. Clay minerals are completely dispersed and contain a large number of micropores [13,53]. Due to mechanical compaction, the shale enters the early diagenetic stage. Pore water is discharged, clay mineral particles have a prismatic shape way, and the shale has high viscosity [21,54]. As the compaction

proceeds, the pore water is drained, and the adsorbed water is slowly discharged in the later stage. The clay particles become dispersed and form flocculates with directionality [55]. Organic matter decomposes due to bacterial action, and biochemical gases are produced, such as pyrite. A small amount of montmorillonite undergoes interlayer collapse due to dehydration and shrinkage and begins to transform into a mixed layer of illite and smectite.

As the compaction continues, the shale enters the middle diagenetic stage. The formation temperature and pressure increase, and the montmorillonite continues to dehydrate, resulting in interlayer collapse [56]. Organic matter generates hydrocarbons in large quantities and produces organic acid, resulting in acidic pore fluid [57]. The unstable components, such as feldspar, are dissolved and release potassium ions. Thus, montmorillonite is rapidly transformed into the illite and smectite mixed layer, which is transformed into illite and releases interlayer water [44]. At this time, pyrite occurs in large quantities. The volume of clay minerals shrinks during the outflow of interlayer water, causing shrinkage joints in the shale [34,55]. The shale is rigidly consolidated in the later stage. The fluid released during the transformation of clay minerals and the thermal evolution of organic matter cannot be discharged. Thus, cracks are formed due to excessive pore fluid pressure and tectonic stress, forming seepage channels. The precipitation of authigenic minerals, such as gypsum, quartz, or iron calcite, occurs due to the maturation of organic matter and the weakening of the pore fluid's acidity (Figure 12).
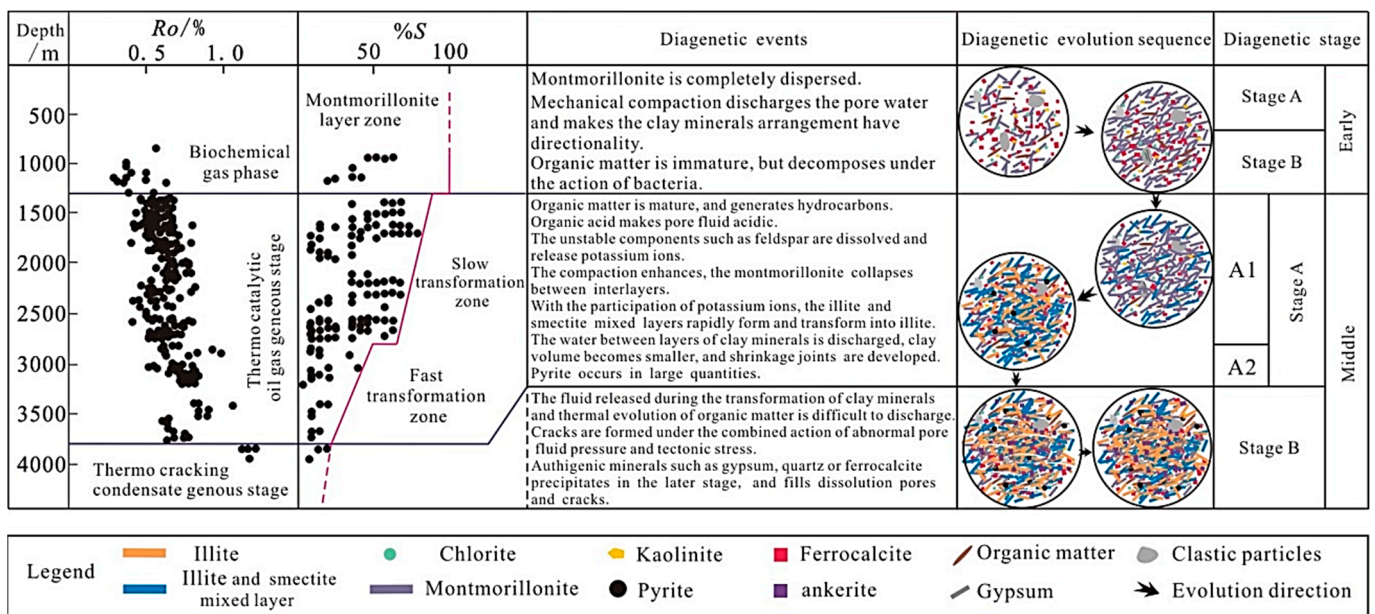

Figure 12. The diagenetic evolution model of the E1f2 shale.

5.3. Pore Evolution of Shale

The diagenetic events and pore evolution are assessed based on the transformation of the shale reservoir space during diagenesis [58] (Figure 13). In the early diagenetic stage, shale diagenesis is dominated by mechanical compaction, and the reservoir space consists of clastic grains and mineral intercrystalline pores. As the mechanical compaction continues and the intermediate diagenetic stage A is entered, the number of primary pores decreases, and the organic matter begins to generate hydrocarbons [59]. The organic matter produces organic pores, and the pore fluid becomes acidic. Unstable components, such as calcite and feldspar, are dissolved, resulting in dissolution pores [60]. Sulfide is generated, enriching pyrite, and pyrite intercrystalline pores are generated. The interlayer water of clay minerals is removed during the transformation, and the volume of clay minerals shrinks, resulting in shrinkage joints [35]. Therefore, dissolution pores and fractures are the most important reservoir types in the middle diagenetic stage A, followed by organic pores and mineral intercrystalline pores. In the middle diagenetic stage B, organic matter

evolves to the highest maturity, and numerous organic-matter pores appear, representing the dominant reservoir space in this stage. Solution pores and fractures are still critical reservoir spaces, but they are often completely or semifilled by authigenic minerals, such as gypsum, quartz, or iron calcite.
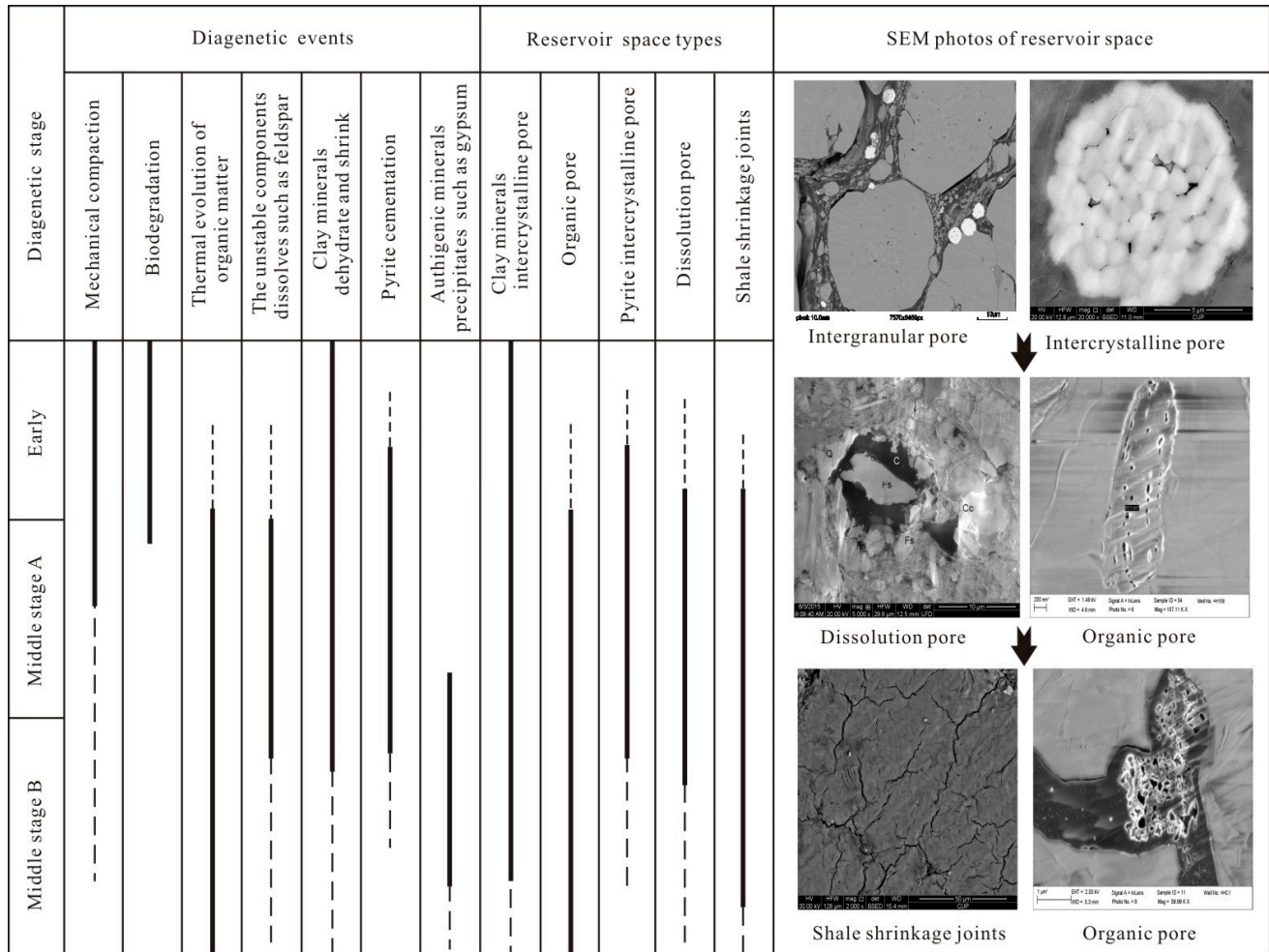

Figure 13. The diagenesis events and the pore evolution of the E_1f_2 shale.

6. Conclusions

(1) The shale diagenesis types in the second member of the Funing Formation (Fu-2) in the Subei Basin included compaction, dissolution, cementation, metasomatism, dolomitization, dehydration/shrinkage, transformation of clay minerals, and thermal evolution of organic matter.

(2) The diagenetic stages of shale were determined by considering the thermal evolution of organic matter and the transformation of clay minerals. The middle diagenetic stage A is dominant in the Fu-2 in the Subei Basin; some parts of the formation are in the early diagenetic stage B and the middle diagenetic stage B.

(3) A diagenetic evolution model of the shale in the Fu-2 in the North Jiangsu Basin was established by considering the diagenetic changes in organic matter maturity and the contents of the clay, clastic, and carbonate minerals during diagenesis. The diagenetic evolution sequences included interlayer collapse and shrinkage of montmorillonite in the early stage; rapid formation and transformation of mixed layers, massive hydrocarbon generation and dissolution of unstable components of organic matter in the middle stage; and fracture generation and filling by authigenic minerals, such as gypsum, quartz, or iron calcite in the later stage.

(4)   The diagenetic events and pore evolution of the Fu-2 were summarized. Primary intergranular pores and mineral intercrystalline pores were the dominant reservoir spaces during early diagenesis. Solution pores and fractures were the most prevalent in the middle diagenetic stage A, followed by organic pores and mineral intercrystalline pores. Organic pores were the main reservoir spaces in the middle diagenetic stage B. Dissolution pores and fractures still represented key reservoir spaces, but many were completely or semifilled by authigenic minerals, such as gypsum, quartz, or iron calcite.

References

1.   Zheng, X.; Pang, M. *Study on Diagenesis of Clastic Reservoir Rocks*; China University of Geosciences Press: Beijing, China, 1989.

2.   Liu, J.; Lai, X.; Yu, B.; Chen, X.; Sui, C. The current situation and developing tendency of the study on diagenesis. *Pet. Geol. Exp.* **2006**, *28*, 65–72.

3.   Quasim, M.A.; Khan, S.; Srivastava, V.K.; Ghaznavi, A.A.; Ahmad, A.H.M. Role of cementation and compaction in controlling the reservoir quality of the Middle to Late Jurassic Sandstones, Jara dome, Kachchh Basin, western India. *Geol. J.* **2021**, *56*, 976–994. [CrossRef]

4.   Dong, D.; Zou, C.; Li, J.; Wang, S.; Li, X.; Wang, Y.; Li, D.; Huang, J. Resource potential, exploration and development prospect of shale gas in the whole world. *Geol. Bull. China* **2011**, *30*, 324–336.

5.   Slatt, R.M.; O'Brien, N.R. Pore types in the Barnett and Woodford gas shales: Contribution to understanding gas storage and migration pathways in fine-grained rocks. *AAPG Bull.* **2011**, *95*, 2017–2030. [CrossRef]

6.   Yang, Y.; Zhang, L.; Feng, Q. Black rock series from the early cambrian Hetang formation in Zhitang Section, west Zhejiang province. *Geol. Sci. Technol. Inf.* **2012**, *31*, 110–117.

7.   Milliken, K.L.; Rudnicki, M.; Awwiller, D.N.; Zhang, T. Organic matter-hosted pore system, Marcllus Formation (Devonian), Pennsylvania. *AAPG Bull.* **2013**, *97*, 177–200. [CrossRef]

8.   Zhao, J.; Feng, Z.; Yang, D.; Kang, Z. Study of pyrolysis and internal structural variation of oil shale based on 3D CT images. *Chin. J. Rock Mech. Eng.* **2014**, *33*, 112–117.

9.   Milliken, K.L.; Esch, W.L.; Reed, R.M.; Zhang, T. Grain assemblages and strong diagenetic overprinting in siliceous mudrocks, Barnett Shale (Mississippian), Fort Worth Basin, Texas Properties of Siliceous Mudrocks, Barnett Shale, Texas. *AAPG Bull.* **2012**, *96*, 1553–1578. [CrossRef]

10.   Aplin, A.C.; Macquaker, J.H.S. Mudstone diversity: Origin and implication for source, seal and reservoir properties in petroleum system. *AAPG Bull.* **2011**, *95*, 2031–2059. [CrossRef]

11.   Lu, L.; Liu, W.; Wei, Z.; Pan, A.; Zhang, Q.; Teng, G. Diagenesis of the Silurian Shale, Sichuan Basin: Focus on pore development and preservation. *Acta Pet. Sin.* **2022**, *40*, 73–87.

12.   Zhao, J.; Jin, Z. Mudstone diagenesis: Research advances and prospects. *Acta Pet. Sin.* **2021**, *39*, 58–72.

13.   Potter, P.E.; Maynard, J.B.; Depetris, P.J. Mud and Mudstone: Introduction and Review. *Clay Clay Miner.* **2005**, *53*, 550–552.

14.   Huang, Z.; Guo, X.; Liu, B.; Zhang, D.; Zhang, J.; Qi, Y.; Wang, R. The Reservoir Space Characteristics and Origins of Lucaogou Formation Source Rock Oil in the Malang Sag. *Acta Sedimentol. Sin.* **2012**, *30*, 1115–1122.

15.   Jiang, Z.; Liang, C.; Wu, J.; Zhang, Z.; Zhang, W.; Wang, Y.; Liu, H.; Chen, X. Several issues in sedimentological studies on hydrocarbon-bearing fine-grained sedimentary rocks. *Acta Pet. Sin.* **2013**, *34*, 1031–1039.

16.   Milliken, K.A. Compositional classification for grain assemblages in fine-grained sediments and sedimentary rocks. *J. Sediment. Res.* **2014**, *84*, 1185–1199. [CrossRef]

17.   Dong, C.; Ma, C.; Luan, G.; Lin, C.; Zhang, X.; Ren, L. Pyrolysis simulation experiment and diagenesis evolution pattern of shale. *Acta Pet. Sin.* **2015**, *33*, 1053–1061.

18. Camp, W.K.; Milliken, K.L.; Fishman, N.S.; Hackley, P.C. Depth of burial for lithification and diagenesis of muds and sands on early Mars. In Proceedings of the SEPM-AAPG Mudstone Diagenesis Hedberg Research Conference Summary, Santa Fe, NM, USA, 16–19 October 2016.
19. Beloborodov, R.; Pervukhina, M.; Luzin, V.; Delle Piane, C.; Clennell, M.B.; Zandi, S.; Lebedev, M. Compaction of quartz-kaolinite mixtures: The influence of the pore fluid composition on the development of their microstructure and elastic anisotropy. *Mar. Pet. Geol.* **2016**, *78*, 426–438. [CrossRef]
20. Goulty, N.R.; Sargent, C.; Andras, P.; Aplin, A.C. Compaction of diagenetically altered mudstones—Part 1: Mechanical and chemical contributions. *Mar. Pet. Geol.* **2016**, *77*, 703–713. [CrossRef]
21. Van de Kamp, P.C. Smectite-illite-muscovite transformations, quartz dissolution, and silica release in shales. *Clays Clay Miner.* **2008**, *56*, 66–81. [CrossRef]
22. Peltonen, C.; Marcussen, Ø.; Bjørlykke, K.; Jahren, J. Clay mineral diagenesis and quartz cementation in mudstones: The effects of smectite to illite reaction on rock properties. *Mar. Pet. Geol.* **2009**, *26*, 887–898. [CrossRef]
23. Baruch, E.T.; Kennedy, M.J.; Löhr, S.C.; Dewhurst, D.N. Feldspar dissolution-enhanced porosity in Paleoproterozoic shale reservoir facies from the Barney Creek Formation (McArthur Basin, Australia). *AAPG Bull.* **2015**, *99*, 1745–1770. [CrossRef]
24. Macquaker, J.H.; Taylor, K.G.; Keller, M.; Polya, D. Compositional controls on early diagenetic pathways in fine-grained sedimentary rocks: Implications for predicting unconventional reservoir attributes of mudstones. *AAPG Bull.* **2014**, *98*, 587–603. [CrossRef]
25. Camp, W.K. Diagenetic evolution of organic matter cements in unconventional shale reservoirs. In Proceedings of the AAPG 2015 Annual Convention and Exhibition, Denver, CO, USA, 31 May–3 June 2015.
26. Wu, L.; Li, X.; Guo, X.; Luo, Q.; Liu, X.; Chen, X.; Jiang, Z. Diagenetic evolution and formation mechanism of dissolved pore of shale oil reservoirs of Lucaogou formation in Malang sag. *J. China Univ. Pet. Ed. Nat. Sci.* **2012**, *36*, 38–43.
27. Dong, C.; Ma, C.; Lin, C.; Sun, X.; Yuan, M. A method of classification of shale set. *J. China Univ. Pet. Ed. Nat. Sci.* **2015**, *39*, 1–7.
28. Zhang, S.; Liu, H.; Wang, M.; Fu, A.; Bao, Y.; Wang, W.; Teng, J.; Fang, Z. Pore evolution of shale oil reservoirs in Dongying Sag. *Acta Pet. Sin.* **2018**, *39*, 754–766.
29. Macquaker, J.H.; Curtis, C.D.; Coleman, M.L. The role of iron in mudstone diagenesis; comparison of Kimmeridge Clay Formation mudstones from onshore and offshore (UKCS) localities. *J. Sediment. Res.* **1997**, *67*, 871–878.
30. Milliken, K.L.; Ergene, S.M.; Ozkan, A. Quartz types, authigenic and detrital, in the upper cretaceous eagle ford formation, South Texas, USA. *Sediment. Geol.* **2016**, *339*, 273–288. [CrossRef]
31. Zhu, Y.; Li, S.; Pan, R.; Tan, M.; Chen, H.; Wang, X.; Chen, F.; Zhang, M.; Hou, B.; Dong, Y. Hotspots and progress in sedimentology: A review of the 32nd international sedimentology conference. *Chin. J. Palaeogeogr.* **2016**, *18*, 699–716.
32. Kokkinos, N.C.; Nkagbu, D.C.; Marmanis, D.I.; Dermentzis, K.I.; Maliaris, G. Evolution of Unconventional Hydrocarbons: Past, Present, Future and Environmental FootPrint. *J. Eng. Sci. Technol. Rev.* **2022**, *15*, 15–24. [CrossRef]
33. Foscolos, A.E.; Kodama, H. Diagenesis of clay minerals from Lower Cretaceous shales of northeastern British Columbia. *Clays Clay Miner.* **1974**, *22*, 319–335. [CrossRef]
34. Bjølykke, K. Clay mineral diagenesis in sedimentary basins-a key to the prediction of rock properties. Examples from the North Sea Basin. *Clay Miner.* **1998**, *33*, 15–34. [CrossRef]
35. Lahann, R.W.; Lahann, W.; McCarty, D.K.; Hsieh, J.C.C. Influence of clay diagenesis on shale velocities and fluid-pressure. In Proceedings of the Offshore Technology Conference, Houston, TX, USA, 30 April–3 May 2001.
36. Wang, X. *Structural and Sedimentary Evolution of Funing Formation in West Slop of Jinhu Sag*; China University of Petroleum (East China): Dongying, China, 2011.
37. Wang, X. *Study on the Sedimentary System of the Third Member of Paleogene Funing Formation in the Subei Basin*; China University of Geosciences (Beijing): Beijing, China, 2017.
38. Pommer, M.; Milliken, K. Pore types and pore-size distributions across thermal maturity, Eagle Ford Formation, southern Texas. *AAPG Bull.* **2015**, *99*, 1713–1744. [CrossRef]
39. Yang, R.; He, S.; Yi, J.; Hu, Q. Nano-scale pore structure and fractal dimension of organic-rich Wufeng-Longmaxi shale from Jiaoshiba area, Sichuan Basin: Investigations using FE-SEM, gas adsorption and helium pycnometry. *Mar. Pet. Geol.* **2016**, *70*, 27–45. [CrossRef]
40. Loucks, R.G.; Reed, R.M.; Ruppel, S.C.; Jarvie, D.M. Morphology, genesis, and distribution of nanometer-scale pores in siliceous mudstones of the Mississippian Barnett Shale. *J. Sediment. Res.* **2009**, *79*, 848–861. [CrossRef]
41. Yang, W.; Zuo, R.; Jiang, Z.; Chen, D.; Song, Y.; Luo, Q.; Wang, Q.; Zhu, H. Effect of lithofacies on pore structure and new insights into pore-preserving mechanisms of the over-mature Qiongzhusi marine shales in Lower Cambrian of the southern Sichuan Basin, China. *Mar. Pet. Geol.* **2018**, *98*, 746–762. [CrossRef]
42. Liu, H.; Zhang, S.; Song, G.; Wang, X.; Teng, J.; Wang, M.; Bao, Y.; Yao, S.; Wang, W.; Zhang, S.; et al. Effect of shale diagenesis on pores and storage capacity in the Paleogene Shahejie Formation, Dongying Depression, Bohai Bay Basin, east China. *Mar. Pet. Geol.* **2019**, *103*, 738–752. [CrossRef]
43. Liang, C.; Cao, Y.; Liu, K.; Jiang, Z.; Wu, J.; Hao, F. Diagenetic variation at the lamina scale in lacustrine organic-rich shales: Implications for hydrocarbon migration and accumulation. *Geochim. Cosmochim. Acta* **2018**, *229*, 112–128. [CrossRef]

44. Makled, W.A.; Mostafa, T.F.; Mousa, D.A.; Abdou, A.A. Source rock evaluation and sequence stratigraphic model based on the palynofacies and geochemical analysis of the subsurface Devonian rocks in the Western Desert, Egypt. *Mar. Pet. Geol.* **2018**, *89*, 560–584. [CrossRef]

45. Li, Q.; Pang, X.; Li, B.; Zhao, Z.; Shao, X.; Zhang, X.; Wang, Y.; Li, W. Discrimination of effective source rocks and evaluation of the hydrocarbon resource potential in Marsel, Kazakhstan. *J. Pet. Sci. Eng.* **2018**, *160*, 194–206. [CrossRef]

46. Staplin, F.L. Sedimentary organic matter, organic metamorphism, and oil and gas occurrence. *Bull. Can. Pet. Geol.* **1969**, *17*, 47–66.

47. Snowdon, L.R. Rock-Eval Tmax suppression: Documentation and amelioration. *AAPG Bull.* **1995**, *79*, 1337–1348.

48. Bray, E.E.; Evans, E.D. Distribution of n-paraffins as a clue to recognition of source beds. *Geochim. Cosmochim. Acta* **1961**, *22*, 2–15. [CrossRef]

49. Lu, J.; Milliken, K.; Reed, R.M.; Hovorka, S. Diagenesis and sealing capacity of the middle Tuscaloosa mudstone at the Cranfield carbon dioxide injection site, Mississippi, USA. *Environ. Geosci.* **2011**, *18*, 35–53. [CrossRef]

50. Ying, F.; He, D. *Diagenesis and Diagenetic Numerical Simulation of Clastic Reservoirs in China's Petroliferous Basins*; Petroleum Industry Press: Beijing, China, 2004.

51. Zhu, J.; Li, S. Study on the diagenesis of clastic oil formation assemblage. *Pet. Geol. Exp.* **1988**, *10*, 223–239.

52. Liu, B.; Zhang, J. *Sedimentary Diagenesis*; Science Press: Beijing, China, 1992.

53. Seely RLiddy, T.J.; Rochelle, C.A.; Fletcher, R.S.; Rigby, S.P. Evolution of the mineralogy, pore structure and transport properties of Nordland Shale following exposure to supercritical carbon dioxide. *J. Pet. Sci. Eng.* **2022**, *213*, 110466. [CrossRef]

54. Metwally, Y.M.; Chesnokov, E.M. Clay mineral transformation as a major source for authigenic quartz in thermo-mature gas shale. *Appl. Clay Sci.* **2012**, *55*, 138–150. [CrossRef]

55. Piper, D.J.W.; Hundert, T.; Pe-Piper, G.; Okwese, A.C. The roles of pedogenesis and diagenesis in clay mineral assemblages: Lower Cretaceous fluvial mudrocks, Nova Scotia, Canada. *Sediment. Geol.* **2009**, *213*, 51–63. [CrossRef]

56. Sun, P.K.; Fang, H.J.; Xu, Z.H.; Wang, C.; Xu, H.M.; Lu, M. Siliciclastic depositional model within a subsurface coastal parasequence based on barriers and baffles—An application to the Donghe Sandstone Member in the Hudson Oilfield, Tarim Basin, NW China. *JPSE.* **2020**, *195*, 107947. [CrossRef]

57. Cavelana, A.; Boussafira, M.; Milbeaua, C.L.; Rozenbaumd, O.; Laggoun-Défarge, F. Effect of organic matter composition on source rock porosity during confined anhydrous thermal maturation: Example of Kimmeridge-clay mudstones. *Int. J. Coal Geol.* **2019**, *212*, 10323. [CrossRef]

58. Garagulya, I.; Vargaa, A.; Raucsika, B.; Schuberta, F.; Czupponb, G.; Frei, R. Pervasive early diagenetic dolomitization, subsequent hydrothermal alteration, and late stage hydrocarbon accumulation in a Middle Triassic carbonate sequence (Szeged Basin, SE Hungary). *Mar. Pet. Geol.* **2018**, *98*, 270–290. [CrossRef]

59. Bitchong, A.M.; Bekono Ottou, J.P.; Bitjong, S.A.; Mandeng, G.N.; Adatte, T. Preliminary source rock evaluation, paleo-depositional environment and hydrocarbon generation potential of the cretaceous organic-rich outcrops of Mayo-Figuil River, Babouri-Figuil Basin, Northern Benue Trough (Yola arm) Cameroon: Insights from bulk geochemistry. *J. Afr. Earth Sci.* **2022**, *192*, 104568.

60. She, M.; Shou, J.; Shen, A.; He, X.; Zhu, Y.; Wang, Y.; Zhang, T. Experimental simulation of dissolution and alteration of buried organic acid fluid on dolomite reservoir. *J. China Univ. Pet. Ed. Nat. Sci.* **2014**, *38*, 10–17.